coatings

MDPI

Article

Exploring the Impact of Spray Process Parameters on Graphite Coating: Morphology, Thickness, and Tribological Properties

Adedoyin Abe[1,2], Josue Goss[1,2] and Min Zou[1,2]

[1] Department of Mechanical Engineering, University of Arkansas, Fayetteville, Arkansas 72701, United States.
[2] Center for Advanced Surface Engineering, University of Arkansas, Fayetteville, Arkansas 72701, United States.

ABSTRACT: This study explores, through a full factorial design of experiment, the effects of graphite concentration and spray flow rate on the morphology, thickness, and tribological performance of graphite coatings for potential tribological applications. Coatings were applied to rough substrates using varying concentrations and flow rates, followed by analysis of their morphological characteristics, roughness, thickness, coefficient of friction (COF), and wear behavior. The results revealed distinct differences in the coating morphology based on flow rate, with low flow rate coatings exhibiting a porous structure and higher roughness, while high flow rate coatings displayed denser structures with lower roughness. Friction as low as 0.09 was achieved which represented an 86% reduction compared to uncoated steel. COF and wear track measurements showed that thickness was influential in determining friction and extent of wear. Flow rate dictated the coating structure, quantity of transfer film on the ball, and the extent of graphite compaction in the wear track to provide a protective layer. SEM and elemental analysis further revealed that graphite coatings provided effective protection against wear, with graphite remaining embedded in the innermost crevices of the wear track. Low flow rates may be preferable for applications requiring higher roughness and porosity, while high flow rates offer advantages in achieving denser coatings and better wear resistance. Overall, this study highlights the importance of optimizing graphite concentration and spray flow rate to tailor coating morphology, thickness, and tribological performance for practical applications.

Keywords: Graphite; spray coating; tribology; design of experiment; solid lubricant; coefficient of friction

Citation: Abe, A.; Goss, J.; Zou, M. Exploring the Impact of Spray Process Parameters on Graphite Coating: Morphology, Thickness, and Tribological Properties. *Coatings* **2024**, *volume number*, x. https://doi.org/10.3390/xxxxx

Academic Editor(s):

Received: date
Accepted: date
Published: date

1. INTRODUCTION

Graphite, an allotrope of carbon, possesses a layered structure where each carbon atom bonds covalently with three others, forming a honeycombed hexagonal lattice. The bonding between the layers is characterized by weak Van der Waals forces, facilitating easy slipping when subjected to shear forces parallel to the lamellar direction. The self-lubricating properties of graphite are useful for various applications, such as release coatings in foundries, additives in lubricating oils, and components of polymer based anti-friction coatings and metal matrix composites [1]–[6]. Graphite is popular as a filler contributing to reduced friction in oils, metal, polymer, and ceramic composites. Despite its effectiveness in these roles, there has been a relative scarcity of tribological research on graphite used as a standalone coating [7]–[10]. This research gap presents an opportunity to explore the tribological performance of spray-coated graphite coating, particularly its potential benefits in reducing friction and wear.

Spray coating is a versatile method for depositing coatings, offering rapid and scalable deposition on various substrates. Understanding the relationship between the resultant coating and the parameters chosen for spraying is crucial across applications [11]–[16].

The design of experiment approach is often chosen due to the complex interaction between several spraying input parameters that influence the output spray and resultant coating [12], [17]. Parameters such as nozzle pressure, air speed, drying temperature, viscosity, distance to substrate, and feed/flow rate directly influence spray dynamics [11], [17]–[21]. Notably, flow rate has been found to significantly affect resultant coating thickness and uniformity [7], [11], [12]. Atomization, the process of breaking a liquid stream into droplets can be expedited using air-assisted atomization. An air atomizing nozzle, which shapes the liquid into a sheet called a fan-spray and then applies air to facilitate atomization, is particularly effective in producing small drop sizes. This method produces smaller droplets compared to no air usage, thus enhancing droplet dispersion for uniform sprays [22]. Researchers have found that the concentration of particle-loaded fluids plays a crucial role in spray dispersion and quality and thus should be carefully chosen [21], [23]–[25]. The relationship between graphite concentration in the spraying solution and coating quality warrants further investigation. Additionally, the effects of flow rate on graphite coatings and their tribological properties remain underexplored.

In this study, we aim to bridge these knowledge gaps by systematically examining the influence of graphite concentration and flow rate on the morphology and tribological behavior of spray-coated graphite coatings. In tribology, coating morphology characterized by roughness and thickness has been shown to influence friction and wear performance [26], [27]. Another important factor is the initial substrate roughness which can impact properties like coating adhesion and lubricant retention [28]. While previous research on graphite coatings has primarily focused on smooth substrates like glass, Si wafer, or polished steel, our study expands this range by using the rough surface finish of rolled steel commonly found in industrial applications, such as conveyor manufacturing, automotive components, and agricultural machinery [15], [16], [29].

Recent work by Morstein et al. demonstrated that graphite coatings on rougher substrates (average roughness, Sa = 0.07 μm) outperformed those on smoother surfaces (Sa = 0.01 μm), highlighting the benefits of higher substrate roughness [26] . Furthermore, while the 0.2 μm coatings showed lower friction, they also demonstrated quicker wear compared to the 17 μm coatings, suggesting the potential benefits of investigating coatings with thicknesses beyond these for improved durability [26]. In our study, we investigate the use of substrates with significantly higher average roughness (Sa = 3.5 μm) and coatings with increased thickness outside the previously explored ranges, to further improve performance [30].

Our study investigates the morphology and thickness of sprayed graphite coatings through a full factorial design of experiment, varying graphite concentration and air-assisted spray flow rate. We assess the tribological performance of the resultant coatings to uncover wear mechanisms. This research provides insights into the optimal process parameters required to achieve uniform and effective graphite coatings on rough steel surfaces.

2. MATERIALS AND METHODS

2.1. Fabrication

Hot-rolled mild steel (MS) sheets (ASTM 1011 Commercial Steel, CS Type B) in their original finishing were provided by Hytrol Conveyor Company. The MS was laser cut from 12-gauge stock into 38.1 mm diameter round substrates. The substrates were cleaned in an ultrasonic bath for an hour by immersion in acetone and dried with nitrogen gas. The average roughness of the MS substrates is 3.55 ± 0.25 μm, measured using a laser scanning confocal microscope (Keyence VK-X260).

Aqueous graphite dispersion (AMLube 1127), donated by AML industries, which contains 25% graphite solids was used. The graphite was diluted from 25% to 20%, 10% and 5% vol. solids concentrations using deionized water. The various concentrations were then placed in a shaker mill/ high-energy ball mill (SPEX TM 8000D-115 Mixer/Mill) for an hour with SPEX ball set (two 12.7 mm and four 6.35 mm hardened 440C stainless steel

balls). The dispersions were then passed through a 40-micron nylon mesh filter and sprayed onto the cleaned MS substrates.

A custom spray coater booth was utilized for the spray coating process. A Lumina® ST-5 spray nozzle featuring a 1 mm diameter opening was used, configured to a fan spray pattern. The nozzle was positioned 20 cm above the surface and traveled over a distance of 50 cm to ensure even distribution of the spray volume. Air pressures for the air actuated spray were 0.35 ± 0.026 MPa. The total volume of graphite dispersion sprayed for all sample types was 10 mL. Flow rate was controlled by revolving the nozzle knob, adjusting the volume of liquid uptake into the nozzle chamber for spraying onto the samples. The number of revolutions was used to determine low, medium, and high levels of flow rate. The nozzle flow rate range is 0 - 210 mL/min. Measurement of the flow rate with water at 0.35 MPa revealed that 15, 51, and 60 mL/min corresponded to the low, medium, and high levels.

A full factorial design of experiment was employed which varied the graphite concentrations and flow rate factors as seen in Table 1. Three samples of graphite coating were made for each experimental run. Coatings of 5%, 10%, 20%, and 25% vol. graphite dispersion were created from the 25% as received concentration and sprayed at low, medium, and high flow rates. Sprayed coatings were then heated on a hot plate at 120°C for 2 minutes followed by heating in a furnace at 200°C for 4 minutes. The samples were taken out of the furnace and allowed to cool down on a ceramic plate.

Table 1. Full factorial design of experiment to examine the effects of flow rate and graphite concentration on the sprayed graphite coatings.

Full Factorial Design		
Run	**Flow Rate**	**Graphite Concentration**
1	low flow rate	5%
2	low flow rate	10%
3	low flow rate	20%
4	low flow rate	25%
5	medium flow rate	5%
6	medium flow rate	10%
7	medium flow rate	20%
8	medium flow rate	25%
9	high flow rate	5%
10	high flow rate	10%
11	high flow rate	20%
12	high flow rate	25%

2.2. Sample characterization

Thickness and roughness measurements of the resultant coatings were carried out on a laser scanning confocal microscope (VK-X260, Keyence Corporation). A step height measurement was used to determine the coating thickness by comparing the average height inside and outside an area where the coating had been scratched off. Area-based observation was preferred over profile measurements due to its higher point density, enhancing accuracy. A scanning electron microscope, VEGA3 SEM (TESCAN OSRAY HOLDING, a.s.) was used to observe the various graphite coating surfaces at different magnifications. For accurate comparison, the view fields were kept consistent across all samples. The SEM images were captured using a 10 kV accelerating voltage, a scan speed of 32 μs/pixel, and a working distance of 16 mm.

2.3. Tribology

Wear tests were performed using a tribometer (UMT-3, Bruker, Inc.) in a ball-on-disk configuration. The 5% and 25% graphite coatings sprayed at low and high flow rates were

selected because coatings deposited at medium flow rate are very similar to the coatings deposited at high flow rate. Tests were repeated for a total of 3 tests per group. Chrome steel balls of 6.35 mm diameter were used in linear reciprocating tests performed at a stroke length of 5 mm, a normal load of 5 N (corresponding to 1.12 GPa Hertzian contact pressure without considering the coating), and at 1 mm/s (0.1 Hz) speed. The ball counterface was thoroughly cleaned with acetone prior to wear testing and imaged using the laser scanning confocal microscope before and after wear testing. The normal and friction forces were measured during the experiment at a sampling rate of 100 Hz. For reference, the same experiment was conducted on mild steel substrates without coating.

2.4. Wear Analysis

The resulting wear tracks and counterface balls were imaged using the laser scanning confocal microscope. Wear analysis was performed by measuring the volume of the wear track using the microscope's Multifile Analysis software. The average depth and width of the wear track were also analyzed. SEM micrographs were captured at different surface locations on the samples to study the microscale topography of the coated surface and the wear tracks. Further elemental analysis of the coatings and wear tracks was performed using an SEM (FEI Nova 600 Nanolab) with Energy Dispersive X-Ray Spectroscopy (EDS). The EDS was used to examine the elemental composition of the wear track and the graphite coating and to confirm the presence of graphite in the wear track after the rubbing interaction.

3. RESULTS AND DISCUSSION

3.1. Coating Morphology, Thickness, and Roughness

Figure 1a presents the graphite coatings obtained at various combinations of graphite concentrations and spray coating flow rates. Visual inspection discerned notable disparities in graphite morphology across the sample groups. The appearance of graphite flakes in the deposited coatings varied throughout the design of experiment range. Coatings produced at low flow rates exhibit porous aggregates of graphite particles arranged hierarchically, while those at medium and high flow rates display flatter topographies. Arrows in Figure 1a indicate areas of uneven coating coverage at a 5% concentration and high flow rate. This likely stemmed from high spray flow rate coupled with the low graphite concentration in the dispersion which corresponded to a dispersion with a high aqueous to solid ratio. In this scenario, the dispensing nozzle causes the graphite dispersion to form large droplets which pool on the surface. Consequently, during the drying process, liquid is drawn away from the droplet edges resulting in uncoated gaps in the coated surface, indicated by arrows on the figure. Conversely, when the 5% concentration dispersion was sprayed using the low flow rate, the gradual release during each spray facilitated the evaporation of some water from the atomized droplets. Consequently, mostly graphite flakes reached the surface in small aggregates, with the graphite flakes orienting themselves randomly within the aggregates, resulting in bulbous arrangements on the surface. The increase in concentration amounted to larger aggregates in the atomized droplets, thereby forming larger structures on the surface.

Figures 1b and 1c illustrate the averaged roughness and thickness of graphite coatings, respectively, sprayed at different flow rates and concentrations with 10 mL graphite dispersion. Notably, in the low flow rate group, roughness increases with concentration, ranging widely from 8 to 37 μm. On the other hand, in the medium and high flow rate groups, roughness is similar, typically below 4 μm, as evidenced by the flatter nature of the coatings in Figure 1a. Medium and high flow rates facilitated greater deposition of the graphite dispersion during each application, resulting in a wetter substrate surface. In this liquid state, prior to drying, flakes align parallel to the substrate under surface tension, forming uniform films that transition into flat coatings upon drying.

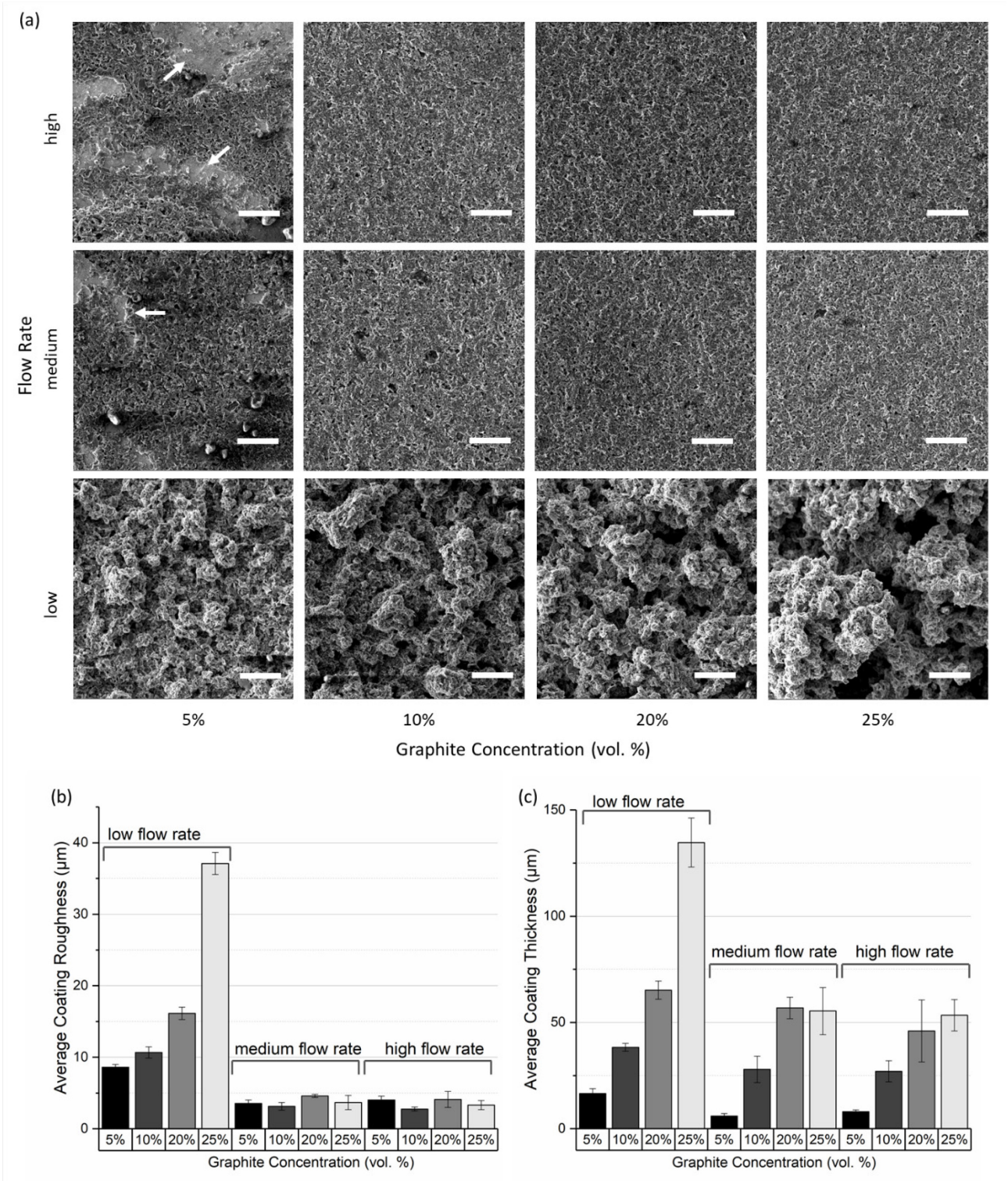

Figure 1. Sprayed graphite coatings on as-received mild steel substrates created at various concentrations and flow rates. (a) Scanning electron microscope (SEM) images of coating surfaces at 250 µm view field. Scalebar = 50 µm (b) Coating roughness and (c) thickness.

At medium and high flow rates, the uneven coverage observed at 5% concentration is different from the uniform coatings observed at higher concentrations, attributable to increased solids concentration. Spray coating, being a rapid deposition method, readily allows for thickness augmentation. As depicted in Figure 1c, thickness increases with rising graphite concentration. The higher solids content at elevated concentrations leaves a greater graphite portion on the surface post-drying compared with lower concentrations, thereby augmenting coating thickness. Due to the random orientation of graphite in low

flow rate coatings, thicknesses tend to be higher than the medium and high flow rate coatings because of increased porosity.

The contour plots in Figure 2a and 2b depict variations in roughness and thickness map, respectively, as a function of graphite concentration and spray flow rate. These figures offer a visual representation of the data presented in Figures 1b and 1c, with the Y axis scaling reflecting the measured flow rates. However, it's important to note that adjusting the nozzle knob changes the chamber size nonlinearly. One, two, and three revolutions corresponded to flow rates of 15, 51, and 60 mL/min for low, medium, and high levels, respectively. Consequently, the medium and high flow rates are relatively closer in value compared to the medium to low flow rate, which explains the similar surface roughness of the coatings deposited at medium and high flow rate.

Two-way analysis of variance (ANOVA) with replication was conducted on our full factorial design to assess the impact of graphite concentration and spray flow rate on both roughness and thickness responses. Replication refers to having multiple measurements for each combination of factor levels. ANOVA calculates F-values to test the significance of each factor and their interactions. To determine whether the observed F-value is statistically significant, we compared it to a critical value from the F-distribution. This critical value depends on the number of levels in each factor as well as the level of significance (α = 0.05). If the calculated F-value exceeds the critical F-value, it suggests that the observed differences between group means are statistically significant. Flow rate, graphite concentration and their interaction had critical F-values of 3.4, 3.0, and 2.5, respectively. A low p-value (below the chosen significance level of 0.05) suggests that the observed differences between group means are unlikely to be due to random chance, leading to rejection of the null hypothesis. P-values provide a simple indication of significance and are used in conjunction with F-values to assess the statistical significance of the observed results.

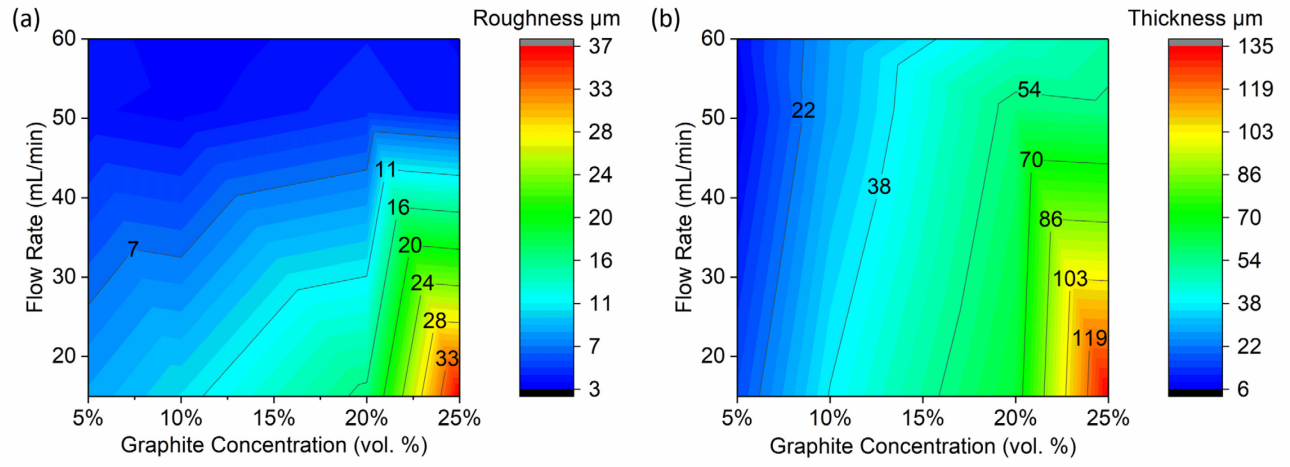

Figure 2. Contour plots showing the change in roughness and thickness at various graphite concentrations and spray flow rates. (a) roughness and (b) thickness.

For the roughness response, simple main effects analysis demonstrated that both flow rate ($F = 1352$, $p = 2.14 \times 10^{-25}$) and graphite concentration ($F = 276$, $p = 1.01 \times 10^{-18}$) had statistically significant effects on roughness. Also, analysis revealed a statistically significant interaction between the effects of graphite concentration and spray flow rate ($F = 275$, $p = 6.70 \times 10^{-21}$). Similarly, examining the thickness response, the two-way ANOVA identified statistically significant simple main effects of both flow rate ($F = 61$, $p = 3.45 \times 10^{-10}$) and graphite concentration ($F = 159$, $p = 5.79 \times 10^{-16}$). Furthermore, the interaction between the effects of graphite concentration and spray flow rate on thickness was also significant ($F = 22$, $p = 8.82 \times 10^{-9}$). The statistically significant interactions observed in the ANOVA analyses for both roughness and thickness underscore the significance of the interplay between graphite concentration and spray flow rate factors in determining the final morphology and thickness of graphite coatings.

Table 2: Analysis of variance on the influence of concentration and flow rate spray factors on the roughness and thickness response of the resultant graphite coatings.

Roughness						
Source of Variation	**SS**	**df**	**MS**	**F**	**P-value**	**F crit**
Flow Rate	1678.75	2	839.37	1352.27	2.14×10^{-25}	3.40
Concentration	513.10	3	171.03	275.54	1.01×10^{-18}	3.01
Interaction	1023.95	6	170.66	274.94	6.70×10^{-21}	2.51
Within	14.90	24	0.62			
Total	3230.69	35				
Thickness						
Source of Variation	**SS**	**df**	**MS**	**F**	**P-value**	**F crit**
Flow Rate	6605.27	2	3302.63	61.73	3.45×10^{-10}	3.40
Concentration	25505.37	3	8501.79	158.92	5.79×10^{-16}	3.01
Interaction	7271.27	6	1211.88	22.65	8.82×10^{-9}	2.51
Within	1283.95	24	53.50			
Total	40665.85	35				

3.2. Friction

Figure 3 illustrates the coefficient of friction (COF) averaged over the test duration for each group. The measured COF for the mild steel substrate is 0.65 due to steel-on-steel interaction, consistent with values reported in literature [26]. Samples coated with graphite have significantly lower COF of 0.09 to 0.19, which is 71% to 86% smaller than that of uncoated samples. In existing literature, friction of graphite ranges widely from 0.1 to 0.9, dependent on factors such as environment and testing conditions but COF of 0.17 in humid air is widely referenced [31], [32]. Specifically, the 5% concentration coatings exhibited average COF values of approximately 0.1, while the 25% graphite coatings displayed average COF values ranging from 0.15 to 0.19 (Fig. 3).

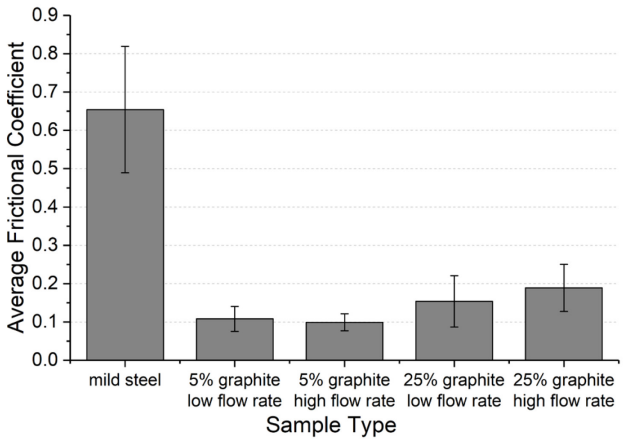

Figure 3. Average coefficient of friction (COF) of mild steel and various graphite coatings tested in linear reciprocating motion against chrome steel counterface balls under a 5 N load at a speed of 1 mm/s.

Figure 4 depicts the COF during each test for all sample groups. The relative differences among all samples are easily seen. Initially, the mild steel substrate exhibits an increasing trend, reaching a COF of about 0.7 at the conclusion of the test. In contrast, the low concentration graphite coatings display a brief run-in period within the first 100 seconds, followed by a reduction to a stable COF of about 0.1, which is maintained throughout the test duration.

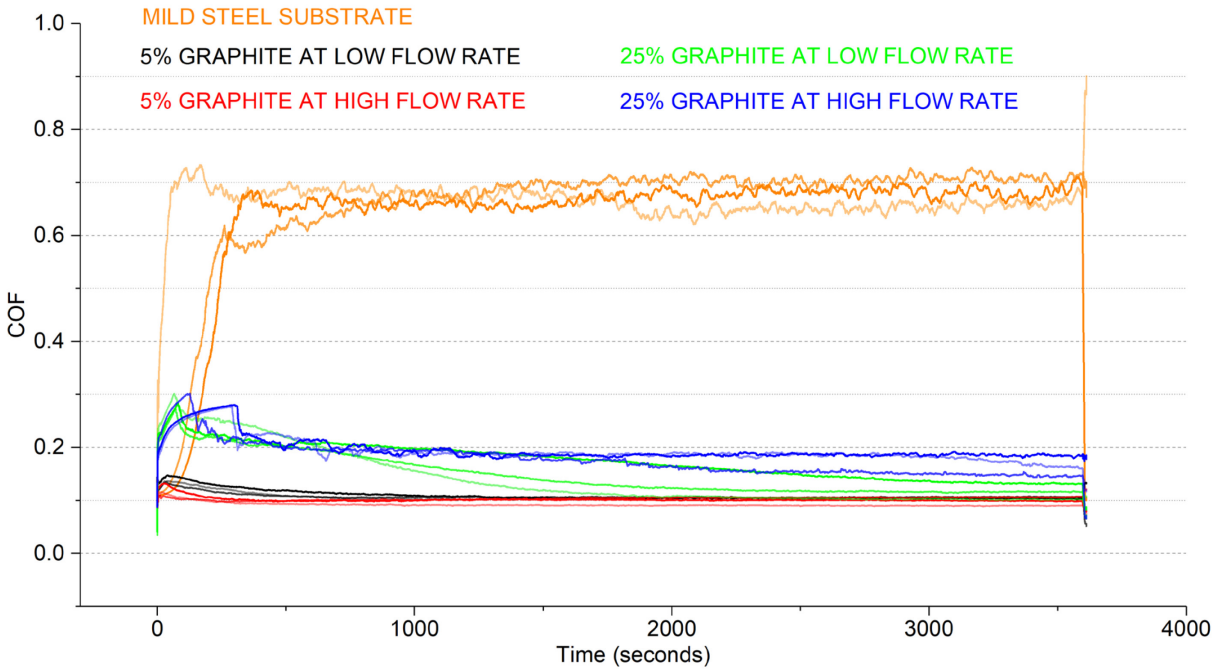

. 8

Figure 4. COF measured during linear reciprocating tests against chrome steel counterface balls under 5 N normal load at 1 mm/s speed for all sample groups.

Research shows that graphite exhibits the lowest friction during perfectly aligned relative motion [8], [33]. However, the high concentration coatings exhibit a different trend from the low concentration coatings. During the run-in period, friction rises to about 0.3, persisting for a longer duration compared to the low concentration coatings. After reaching 0.3, the COF for the high concentration coatings continues to decrease, approaching a COF above 0.1 at the end of the test. This can be attributed to the higher quantity of graphite flakes in the 25% concentration coatings, requiring additional time for compression and formation of a uniform layer compared to the 5% concentration coatings. Furthermore, the coating on the low flow rate samples have high porosity which weakened the coating shear strength, resulting in slightly lower friction than the high flow rate coating. Additionally, transfer film develops on the counterface as the test progresses, contributing to lower COF.

3.3. Wear

Figure 5a presents top-down SEM images of the coatings before and after dry sliding wear test. On the left (Figs. 5a i-v) images, the mild steel substrate and pristine coatings are depicted, while the right (Figs. 5a vi - x) images reveal the wear tracks resulting from testing. For the mild steel substrate, the oxide layer is worn to expose the steel underneath, with a significant amount of wear debris deposited on the side of the wear track. In the post-wear 5% graphite low flow rate sample (Fig. 5a vii), darker compression areas indicate evidence of compacted graphite that was agitated during testing and displaced to different locations. The boxed area and arrow in Figure 5a vii show where compressed coating material has been removed and redeposited, respectively. Similarly, in Figure 5a

viii, the 5% graphite high flow rate sample exhibits compacted light and darker grey areas within the wear track. In the case of the 25% graphite samples, their thickness leads to a wider wear track, resulting in sidewalls of the wear track containing compacted smooth graphite in most areas. The center of the wear track, where the tip of the ball applies the highest pressure, displays uneven coloration because this area has the greatest potential for wear and transfer of coating material to the counterface. However, the 25% high flow rate sample (Fig. 5a x) demonstrates a narrower wear track compared to the 25% low flow rate sample (Fig. 5a ix), because the higher flow rate resulted in a denser coating.

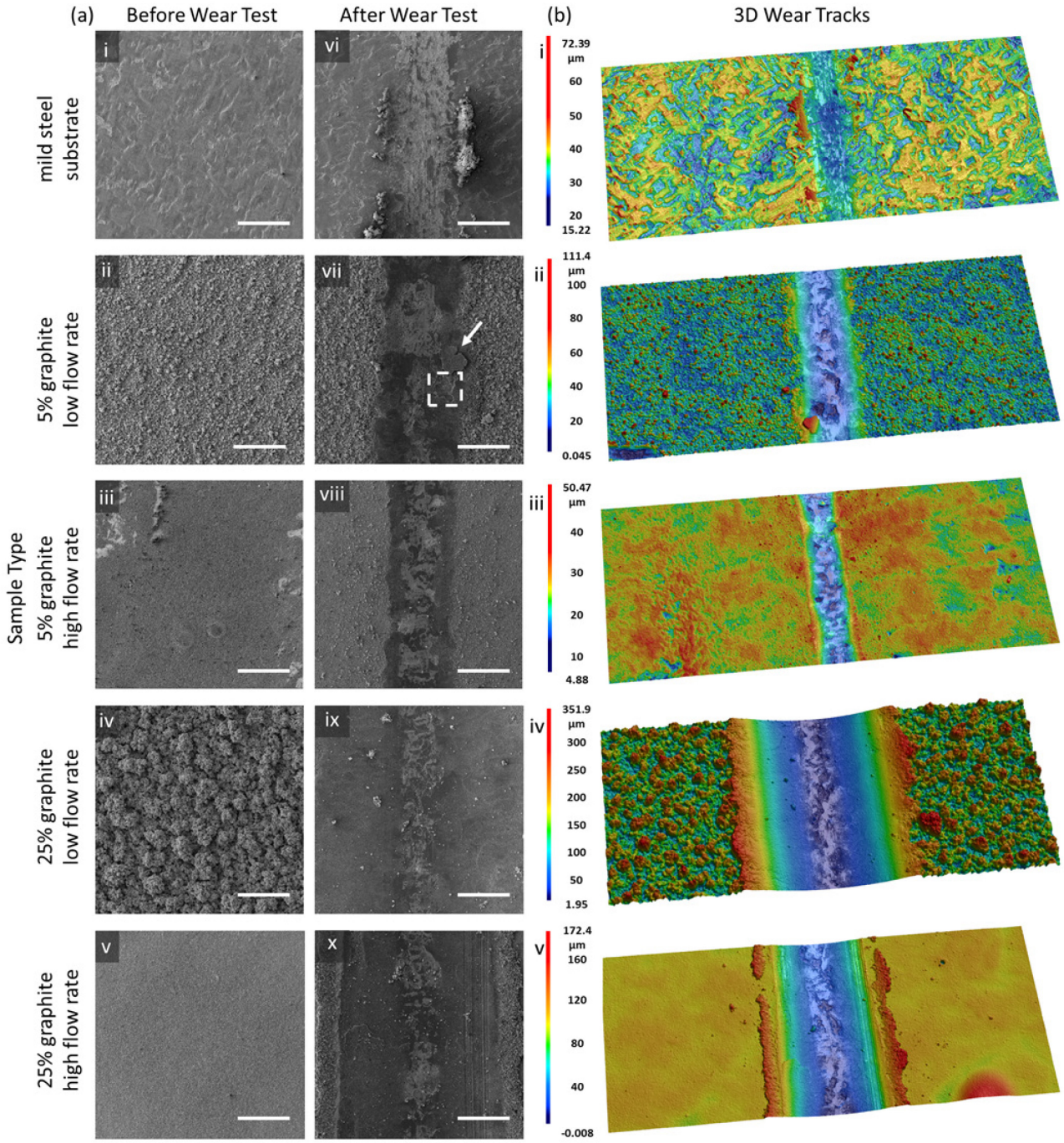

Figure 5. Surface topography before and after wear test. (a) SEM images showing before (left column) and after (middle column) wear tests for mild steel substrate and various graphite coatings. Scalebar = 500 µm. (b) Representative 3D images of wear tracks from Keyence laser scanning confocal microscope showing the z-range and topography difference between samples.

In Figure 5b, representative 3D images of wear tracks for mild steel, 5% graphite and 25% graphite coatings at low and high flow rates are presented, accompanied by their corresponding scale bars. These images showcase the topography of the wear scar and surrounding areas. Notably, the roughness is distinguishable between the uncoated mild steel (Fig. 5b i) and the coated low (Figs. 5b ii and iv) and high (Figs. 5b iii and v) flow rate groups. While the effect of surface roughness on wear performance of graphite coatings has not typically been studied, our observations reveal that apparent lower roughness of the high flow rate samples contribute to narrower wear tracks at both 5% and 25% graphite concentrations due to the compact nature of the graphite coatings helping to resist deformation. This trend is further elucidated in Figure 6.

Figure 6 shows the average wear track volume (a), width (b), and depth (c) of coatings made at low and high flow rates with 5% and 25% graphite concentrations. In Figure 6d, wear track volume, width, and depth are presented relative to coating thickness. Wear track dimensions (volume, width, and depth) in Figures 6 a-c are smaller at high flow rate compared to those at low flow rate. Also, the 5% graphite coatings consistently exhibit smaller wear metrics compared to the 25% counterparts, due to their thinner coatings. For all wear track metrics, there is an increasing trend with increasing coating thickness (Fig. 6d). Wear depth increases with the initial coating thickness. The depth of the wear track resulted from both coating compression and material removal. Morphology influences the wear behavior of graphite coatings. The loosely packed low flow rate coatings could facilitate transfer film formation, holding promise in applications requiring easy transfer of graphite. Conversely, the more densely packed, high flow rate coatings exhibit reduced wear (Fig. 6a), possibly due to the enhanced consolidation of graphite particles and the consequent reinforcement of the coating structure after rubbing.

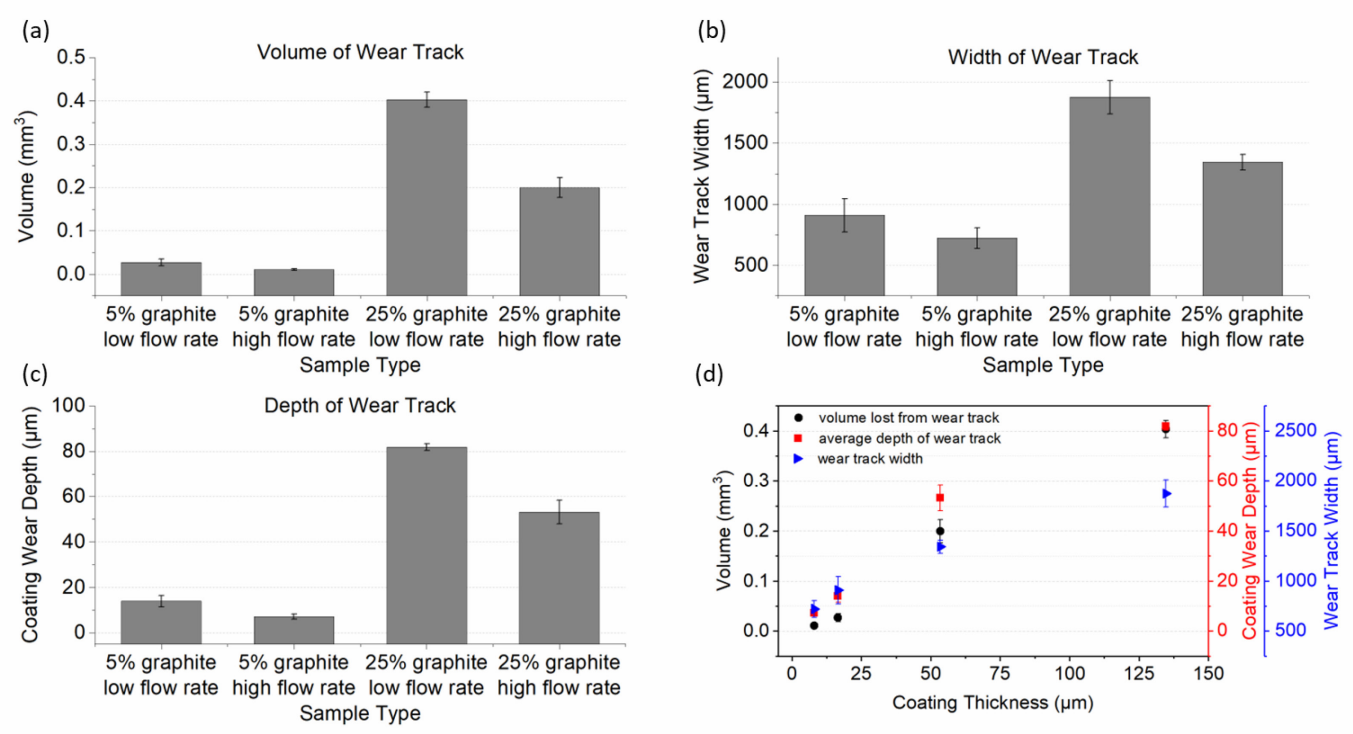

Figure 6. Wear track measurements of 5% and 25% graphite coatings created at low and high flow rates. Average measurements of wear track (a) volume, (b) width, and (c) depth. (d) Comparison of wear track measurements against coating thickness.

Figure 7 illustrates the wear track SEM images and corresponding laser scanning confocal microscope images of balls. Figures 7a and 7b present the wear track and counterface ball on the same scale. The figures are aligned to demonstrate the relative position of the ball during the sliding test. Figures 7c and 7d show higher magnification images of the

ball. In Figure 7a i, the uncoated substrate shows mild steel debris pushed away from the wear track and deposited outside, along with evidence of abrasion within the wear track. The ball rubbed against the mild steel substrate (Fig. 7b i) experienced significant wear, surpassing anything observed on the balls run against the graphite coatings. In contrast, graphite coatings are compressed (Fig. 7a ii-v) during testing and prevent wear on the counterface through the formation of protective films (Fig. 7b ii-v). In the SEM micrographs (Fig. 7a), the compressed graphite coatings exhibit a darker appearance. The area of the ball in contact with the graphite coatings is larger for the thicker 25% coatings compared to the thinner 5% coatings. This is observed by the dark areas on the sides of the ball where it rubbed against the sidewalls of thick coatings (shown with white arrows in Figs. 7c iv and v).

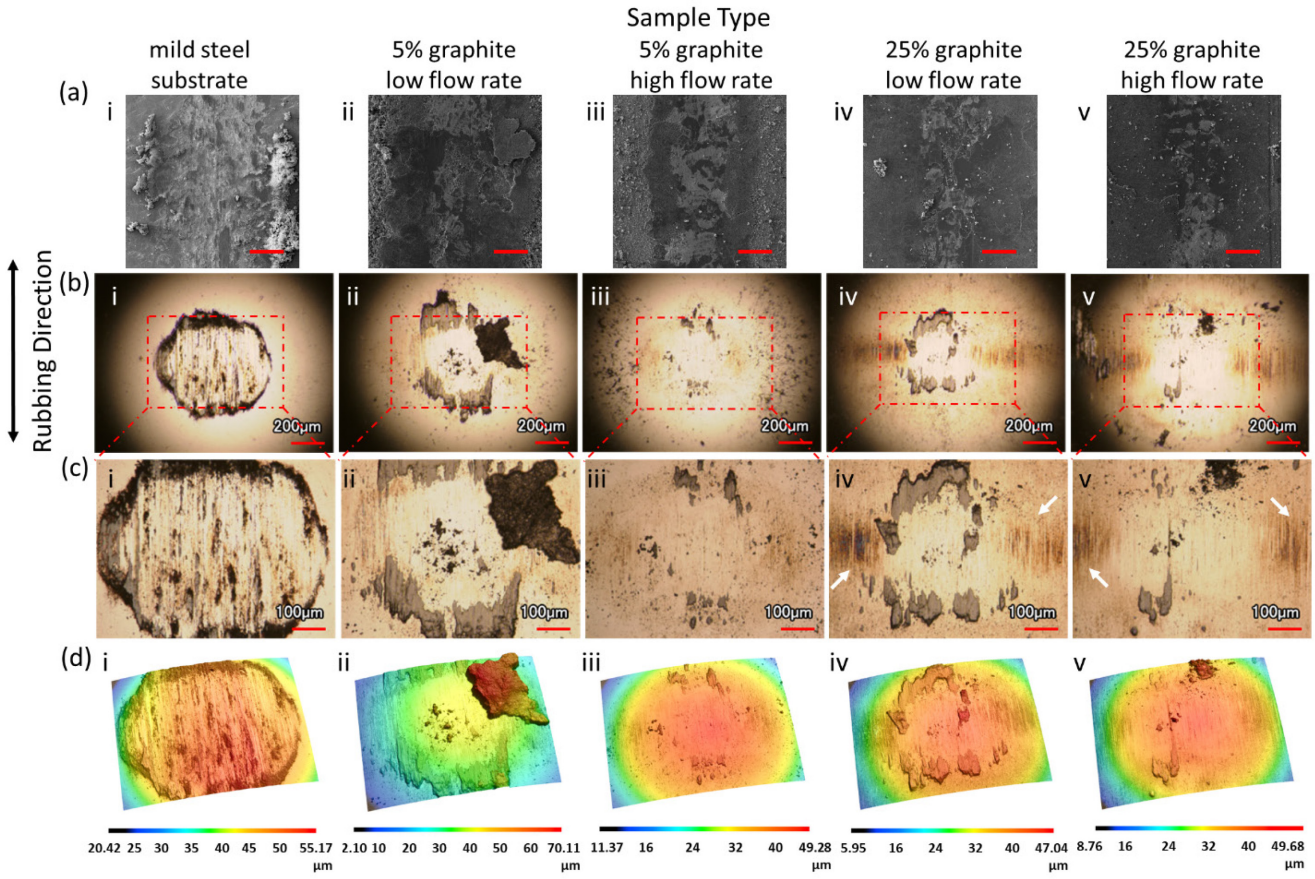

Figure 7. Aligned wear track and ball images after wear tests against mild steel substrates and graphite coatings sprayed at different flow rates and concentrations. (a) Representative SEM images, scalebar = 200 µm aligned with (b) corresponding laser scanning confocal microscope images of counterface ball at 10x, and (c) 20x magnifications. (d) Representative 3D images of balls.

The amount of graphite transferred to each ball varies. In subfigures ii and iv of Figures 7b - d, the low flow rate coatings left substantial wear debris on the ball after rubbing against both 5% and 25% concentration coatings. This is attributed to the porous structure and mobility of graphite flakes of the low flow rate coatings. The high roughness of these coatings also encouraged transfer film formation. In subfigures iii and v of Figures 7b-d, the high flow rate coatings exhibited some transfer films protecting the rubbing interface.

SEM images of the wear tracks from representative tests are presented in Figure 8, where the boxed regions of interest are depicted at progressively higher magnifications in each row. The middle of the wear track represents the highest contact pressure area in the rubbing direction, providing insights into the most severe wear experienced by the coatings. In subfigure i of Figure 8 a-c, the uncoated mild steel shows abrasion lines, debris particles, and uneven surfaces in the wear scar. On the other hand, in subfigures ii-v of

Figure 8 a-c of the coated samples, graphite flakes are compressed to form protective layers on the surface. However, these compressed layers depicted in Figure 8 may experience dislodgement, as indicated by the connected dots in subfigures a ii, a iv, b iv, and c iv. The dots are positioned on the side to indicate the original and current locations of dislodged compressed graphite flakes, identifiable by matching the shapes of the flake edge/perimeter. The low flow rate coatings show evidence of compressed flake displacement. In the circled areas in Figures 8a and 8b, the edges of the smoothened plates of darker compressed graphite terminate with smaller graphite particles. Figures 8a and 8c depict the extent of compressed graphite coverage in the area subjected to the highest contact pressure, in contrast to other regions within the wear track. The variation of light and dark areas in subfigures ii - v of Figure 8 indicate that compression is not uniform throughout the wear track. In general, the 25% graphite coatings (subfigures iv and v) provide a more uniform protective layer of compacted graphite compared to the thinner 5% coatings (subfigures ii and iii). Arrows in Figure 8c show wear lines on top of the graphite surface (subfigures ii-v) and on the severely worn mild steel (subfigure i). The compressed graphite separates the counterface ball from the substrate as shown by the wear lines (arrows in Fig 8c). This protective layer is crucial as it serves as a lubricant reservoir, and over time, the alignment of graphite particles facilitates low friction, as observed in Figure 4.

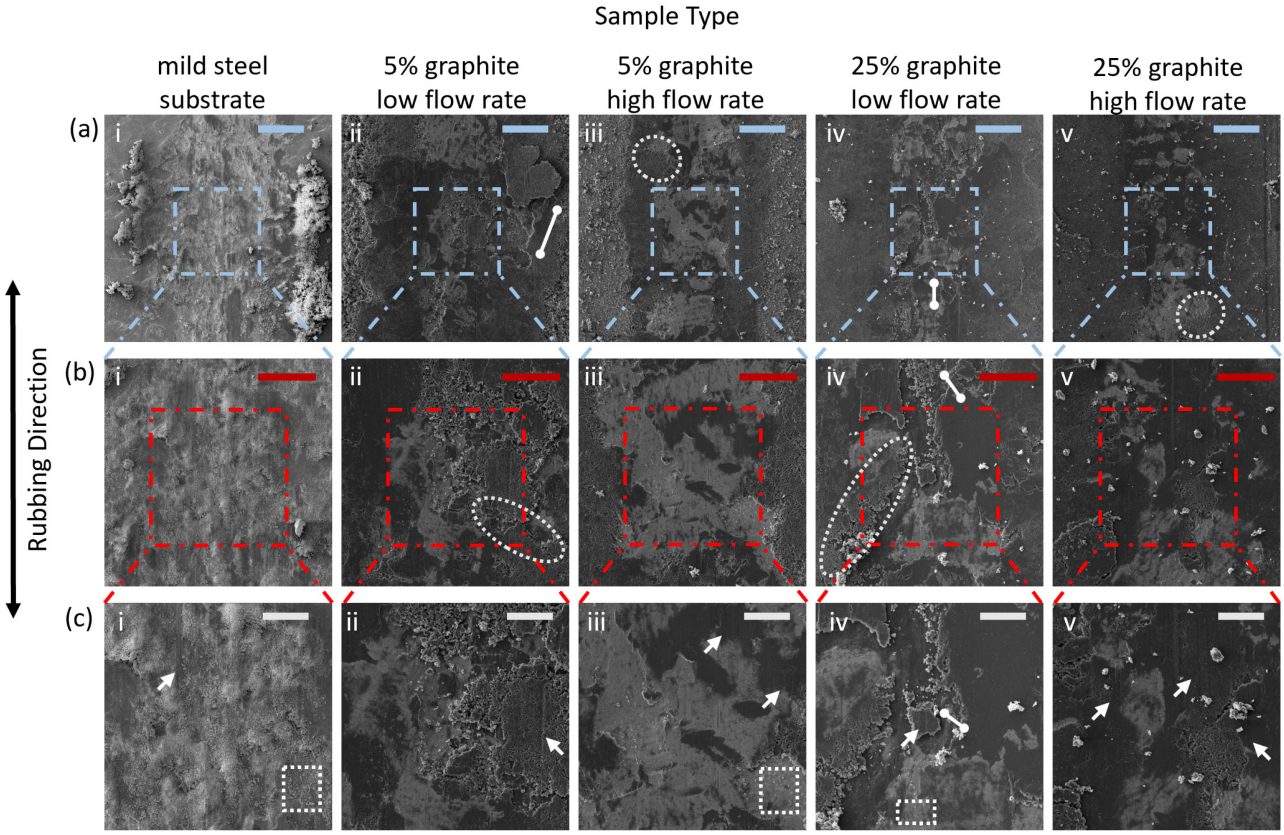

Figure 8. Representative SEM images zooming into the interior portion of the wear tracks. (a) 1000 μm viewfield, Scalebar = 200 μm, (b) 400 μm viewfield, Scalebar = 100 μm, and (c) 250 μm viewfield, Scalebar = 50 μm.

In the innermost portion of the wear track (Fig. 8c), light gray areas sometimes reveal the pebble-like morphology of the underlying mild steel substrate (boxed regions in Figures 8c i, iii and iv). It is unclear if graphite is still present in these small regions. Therefore, elemental analysis of the light areas of the wear track and outside the wear track was carried out at higher magnification and presented in Figures 9 and 10.

3.4. Elemental Analysis

Figure 9a and 9b present SEM images of graphite coatings and the corresponding EDS spectra of these areas. The colors of each group are kept consistent across both Figures 9 and 10. Figure 9a shows the differences in coating morphology between the rough low flow rate coatings (subfigures ii and iv) and the smoother high flow rate coatings (subfigures iii and v). In graphite coatings, carbon (C) is the primary element of interest. Although carbon is also present in mild steel substrates, it constitutes a much smaller percentage, typically less than 0.3%, with iron (Fe) dominating the substrate's spectra. Additionally, manganese (Mn) may be present in mild steel to a lesser extent, and oxygen (O) signals can indicate the presence of ferrous oxides or passivation of dangling bonds in carbon.

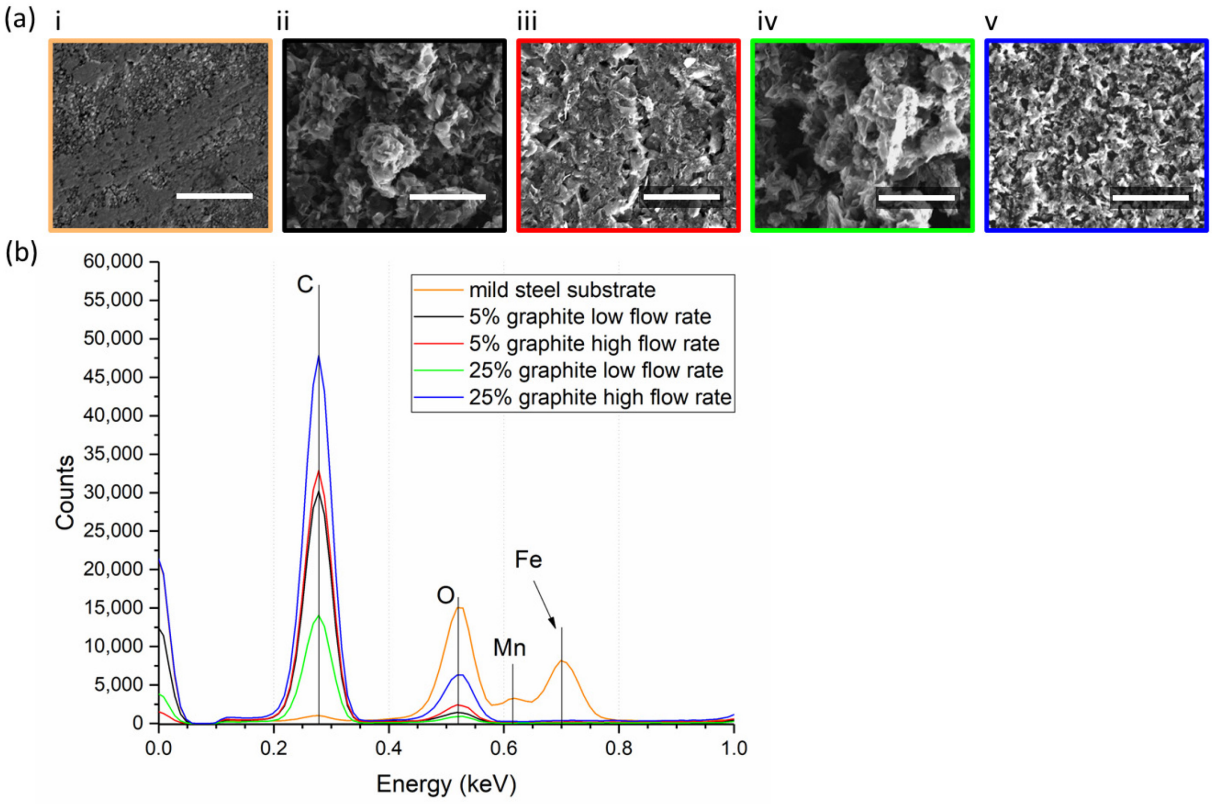

Figure 9. Graphite coating with corresponding EDS spectra (a) SEM images showing graphite coating region (85 μm width at 1500x magnification) Scalebar = 30 μm. (b) EDS spectra of the shown regions.

In Figure 9b, the EDS spectra demonstrates that the 25% low flow rate coatings exhibit the lowest C signal among all coatings. This can be attributed to the high porosity of the region, resulting in fewer graphite flakes penetrated by electrons. Conversely, the 25% high flow rate coating exhibits the strongest C signal for graphite due to its thick and dense coating. As expected, all coatings cover the substrate up to the penetration depth of the electrons, resulting in no Fe signal measured in the graphite coatings, while the mild steel substrate displays high Fe spectra. The mild steel exhibits a high oxygen-to-iron ratio, likely due to the presence of ferrous oxides such as Fe_2O_3 and Fe_3O_4 on the surface.

Figures 10a and 10b present SEM images of the inner portion of the wear track (width of 250 μm, like Figure 8c) and the magnified boxed area, respectively. Their EDS spectra are displayed in Figures 10c and 10d, respectively. In Figure 10a, arrows point to areas of compacted graphite. In Figure 10a and 10c, the analyzed regions show that the 25% low flow rate coating exhibits the highest C signal, which may be influenced by the non-uniform nature of the wear track at this magnification. Nonetheless, the low flow rate samples display significant C counts, indicating good graphite coverage in part of the areas. This suggests that the porous graphite aggregates of the low flow rate coatings are compacted

in the wear track and protect part of the substrate. The mild steel substrate exhibits only low C content, reflecting the minimal carbon contribution of <0.3% in its composition. Importantly, the Fe signal is lower than the respective C signal in all the coatings, indicating sufficient graphite coverage in the wear track.

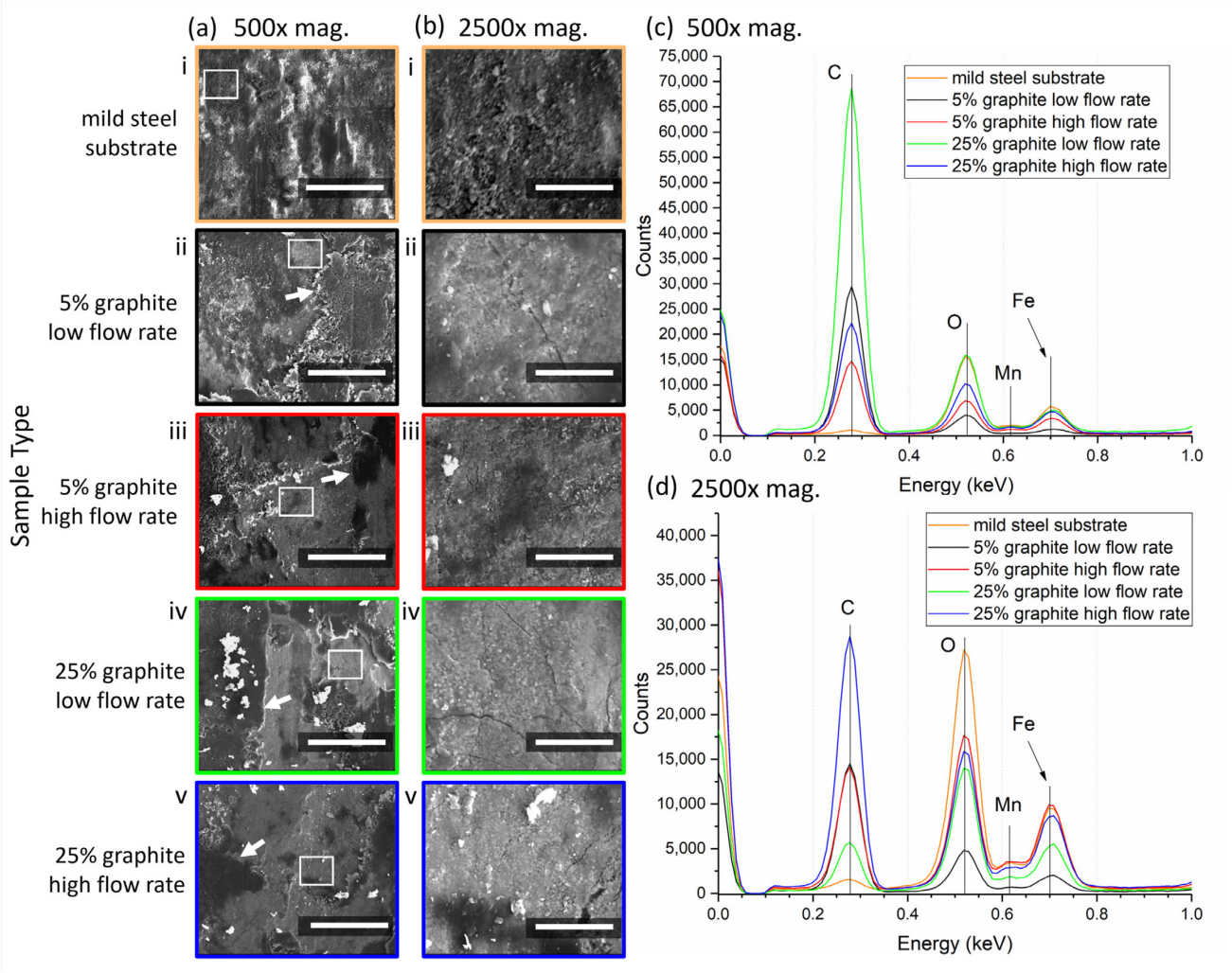

Figure 10. Locations inside wear tracks and their corresponding EDS spectra. (a) SEM images showing wear track inner region (250 μm width at 500x magnification) Scalebar = 100 μm (b) Higher magnification of wear track (50 μm width at 2500x magnification) Scalebar = 20 μm from boxed regions in (a). (c) and (d) EDS spectra corresponding to the interior wear track locations shown in (a) and (b), respectively.

Figure 10b, the zoomed-in grey areas of Figure 10a, show the pebble-like structure of the mild steel and darker grey areas of compressed graphite. EDS spectra in Figure 10d indicate much higher C signals in all coatings than the mild steel, indicating the presence of carbon coating on all coated surfaces. Elemental analysis demonstrates that in the innermost regions of the most worn areas of the wear track, graphite remains embedded in the crevices of the mild steel substrate, contributing to surface protection and low friction.

4. CONCLUSIONS

The surface morphology, coating thickness, and tribological performance of graphite coatings on MS substrates are significantly influenced by both the concentration of graphite dispersion and the spray flow rate. Low flow rate coatings exhibit a porous structure with higher roughness and thicker coating, leading to increased wear track width, depth, and volume. Conversely, high flow rate coatings display a denser structure with lower roughness and thinner coating thickness, resulting in narrower and shallower wear tracks

and reduced wear volume. Both the COF and wear volume of the graphite coatings are mainly affected by the coating thickness, with both increasing with coating thickness. Coating morphology also has some effect on the COF and wear. Rougher and more porous low flow rate coatings require longer time to compact and are easier to shear or remove, resulting in slightly lower COF, more transfer to the ball, and higher wear volume. SEM and EDS analyses reveal that graphite flakes remain embedded in the innermost crevices of the wear track. Despite variations in coating thickness and porosity, all coatings exhibit sufficient coverage in the wear track, contributing to surface protection and low friction. Overall, these findings underscore the importance of optimizing graphite concentration and spray flow rate to tailor coating morphology, thickness, and tribological performance for practical applications. Low flow rates may be preferable for applications requiring higher roughness and porosity, while high flow rates offer advantages in achieving denser coatings with lower roughness and better wear resistance.

Author Contributions: Conceptualization, A.A. and M.Z.; methodology, A.A. and J.G.; formal analysis, A.A.; investigation, A.A.; resources, M.Z.; writing—original draft preparation, A.A.; writing—review and editing, A.A. and M.Z.; visualization, A.A.; supervision, M.Z.; project administration, M.Z.; funding acquisition, M.Z. All authors have read and agreed to the published version of the manuscript.

Funding: This research was funded by the National Science Foundation under Grant Award # 2141026.

Institutional Review Board Statement: Not applicable

Informed Consent Statement: Not applicable

Data Availability Statement: The original contributions presented in the study are included in the article, further inquiries can be directed to the corresponding author.

Conflicts of Interest: The authors declare no conflicts of interest.

Acknowledgments: This work was supported by the National Science Foundation under Grant Award # 2141026. Any opinions, findings, and conclusions or recommendations expressed in this material are those of the authors and do not necessarily reflect the views of the National Science Foundation. We thank Hytrol Conveyor Company and AML Industries for providing the hot-rolled mild carbon steel sheets and aqueous graphite dispersion used in this study, respectively. We also thank the Arkansas Nano-Bio Materials Characterization Facility of the University of Arkansas for equipment use.

REFERENCES

[1] Z. Wang, Q. Fu, and S. Wu, "Effect of solid lubricant particles on the tribological properties of PTFE composites lubricated with natural seawater," *J. Dispers. Sci. Technol.*, vol. 40, no. 2, pp. 239–249, Feb. 2019, doi: 10.1080/01932691.2018.1467774.

[2] S. Ye and X. Zeng, "Tribological properties of PTFE and PTFE composites at different temperatures," *Tribol. Lubr. Technol.*, vol. 70, no. 8, pp. 32–39, 2014, doi: 10.1080/10402004.2013.812759.

[3] R. Wang *et al.*, "Important contributions of carbon materials in tribology: From lubrication abilities to wear mechanisms," *J. Alloys Compd.*, vol. 979, no. January, p. 173454, 2024, doi: 10.1016/j.jallcom.2024.173454.

[4] L. Marcinauskas, J. S. Mathew, M. Milieška, M. Aikas, and M. Kalin, "Effect of graphite concentration on the tribological performance of alumina coatings," *J. Alloys Compd.*, vol. 827, 2020, doi: 10.1016/j.jallcom.2020.154135.

[5] W. Ye *et al.*, "Recent advances in self-lubricating metal matrix nanocomposites reinforced by carbonous materials: A review," *Nano Mater. Sci.*, no. February, 2024, doi: 10.1016/j.nanoms.2024.02.007.

[6] Y. Ren *et al.*, "A review on tribology of polymer composite coatings," *Friction*, vol. 9, no. 3. pp. 429–470, 2021, doi: 10.1007/s40544-020-0446-4.

[7] K. Hanada, K. Hatsukano, K. Matsuzaki, K. Umeda, M. Ishiwata, and M. Tsukita, "Graphite coating of tool steel by pressure spraying," *J. Mater. Process. Technol.*, vol. 164–165, pp. 856–861, 2005, doi: 10.1016/j.jmatprotec.2005.02.171.

[8] R. Buzio, A. Gerbi, C. Bernini, L. Repetto, and A. Vanossi, "Graphite superlubricity enabled by triboinduced nanocontacts," *Carbon N. Y.*, vol. 184, pp. 875–890, 2021, doi: 10.1016/j.carbon.2021.08.071.

[9] T. Cao, Z. Lv, W. Zhang, and W. Zhang, "Preparation and tribological behaviours of graphite self-lubricating

coating deposited on middle carbon steel by electrospark deposition," *Bull. Mater. Sci.*, vol. 45, no. 2, 2022, doi: 10.1007/s12034-022-02682-9.

[10] R. Kumar, I. Hussainova, R. Rahmani, and M. Antonov, "Solid Lubrication at High-Temperatures—A Review," *Materials*, vol. 15, no. 5. Multidisciplinary Digital Publishing Institute, p. 1695, 24-Feb-2022, doi: 10.3390/ma15051695.

[11] M. G. McGrath, A. Vrdoljak, C. O'Mahony, J. C. Oliveira, A. C. Moore, and A. M. Crean, "Determination of parameters for successful spray coating of silicon microneedle arrays," *Int. J. Pharm.*, vol. 415, no. 1–2, pp. 140–149, 2011, doi: 10.1016/j.ijpharm.2011.05.064.

[12] N. Almansoori, S. Aldulaijan, S. Althani, N. M. Hassan, M. Ndiaye, and M. Awad, "Manual spray painting process optimization using Taguchi robust design," *Int. J. Qual. Reliab. Manag.*, vol. 38, no. 1, pp. 46–67, 2021, doi: 10.1108/IJQRM-07-2019-0248.

[13] D. Gleeson *et al.*, "Generating Optimized Trajectories for Robotic Spray Painting," *IEEE Trans. Autom. Sci. Eng.*, vol. 19, no. 3, pp. 1380–1391, 2022, doi: 10.1109/TASE.2022.3156803.

[14] Y. Ren *et al.*, "A review on tribology of polymer composite coatings," *Friction*, vol. 9, no. 3. Springer, pp. 429–470, 28-Nov-2021, doi: 10.1007/s40544-020-0446-4.

[15] I. Juhász Junger *et al.*, "Influence of graphite-coating methods on the DSSC performance," *Optik (Stuttg).*, vol. 174, no. June, pp. 40–45, 2018, doi: 10.1016/j.ijleo.2018.08.041.

[16] L. Chen *et al.*, "Sprayed and mechanical-modified graphite layer as transferred electrode for high-efficiency perovskite solar cells," *Carbon N. Y.*, vol. 202, no. P1, pp. 161–166, 2023, doi: 10.1016/j.carbon.2022.10.075.

[17] J. Karas, S. Pavloková, H. Hořavová, and J. Gajdziok, "Optimization of Spray Drying Process Parameters for the Preparation of Inhalable Mannitol-Based Microparticles Using a Box-Behnken Experimental Design," *Pharmaceutics*, vol. 15, no. 2, 2023, doi: 10.3390/pharmaceutics15020496.

[18] R. V. S. K. Jakkula and P. Sethuramalingam, "Analysis of Coatings based on Carbon-based Nanomaterials for Paint Industries-A Review," *Aust. J. Mech. Eng.*, vol. 21, no. 3, pp. 1008–1036, 2023, doi: 10.1080/14484846.2021.1938953.

[19] M. Barletta and A. Gisario, "Electrostatic spray painting of carbon fibre-reinforced epoxy composites," *Prog. Org. Coatings*, vol. 64, no. 4, pp. 339–349, 2009, doi: 10.1016/j.porgcoat.2008.07.020.

[20] O. Ranta *et al.*, "Quality analysis of some spray parameters when performing treatments in vineyards in order to reduce environment pollution," *Sustain.*, vol. 13, no. 14, 2021, doi: 10.3390/su13147780.

[21] G. H. Kim, E. A. Shin, J. Y. Jung, J. Y. Lee, and C. K. Lee, "Effect of Spray Parameters on Electrical Characteristics of Printed Layer by Morphological Study," *Processes*, vol. 10, no. 5, 2022, doi: 10.3390/pr10050999.

[22] S. Poozesh, N. Akafuah, and K. Saito, "Effects of automotive paint spray technology on the paint transfer efficiency – a review," *Proc. Inst. Mech. Eng. Part D J. Automob. Eng.*, vol. 232, no. 2, pp. 282–301, 2018, doi: 10.1177/0954407017695159.

[23] R. D. Reitz and F. B. Bracco, "On the dependence of spray angle and other spray parameters on nozzle design and operating conditions," *SAE Tech. Pap.*, 1979, doi: 10.4271/790494.

[24] D. Waldbillig and O. Kesler, "The effect of solids and dispersant loadings on the suspension viscosities and deposition rates of suspension plasma sprayed YSZ coatings," *Surf. Coatings Technol.*, vol. 203, no. 15, pp. 2098–2101, 2009, doi: 10.1016/j.surfcoat.2008.11.027.

[25] J. Shi, N. Cagney, J. Tatum, A. Condie, and J. Rafael Castrejon-Pita, "Jetting and droplet formation of particle-loaded fluids," *Phys. Fluids*, vol. 36, no. 1, 2024, doi: 10.1063/5.0180014.

[26] C. E. Morstein and M. Dienwiebel, "Graphite lubrication mechanisms under high mechanical load," *Wear*, vol. 477, no. September 2020, p. 203794, Jul. 2021, doi: 10.1016/j.wear.2021.203794.

[27] S. K. Ghosh, C. Miller, D. Choudhury, J. A. Goss, and M. Zou, "The Effects of PTFE Thickness on the Tribological Behavior of Thick PDA/PTFE Coatings," *https://doi.org/10.1080/10402004.2020.1728001*, vol. 63, no. 3, pp. 575–584, May 2020, doi: 10.1080/10402004.2020.1728001.

[28] C. Miller, D. Choudhury, and M. Zou, "The Effects of Surface Roughness on the Durability of Polydopamine/PTFE Solid Lubricant Coatings on NiTiNOL 60," *Tribol. Trans.*, vol. 62, no. 5, pp. 919–929, 2019, doi: 10.1080/10402004.2019.1641645.

[29] C. E. Morstein, A. Klemenz, M. Dienwiebel, and M. Moseler, "Humidity-dependent lubrication of highly loaded contacts by graphite and a structural transition to turbostratic carbon," *Nat. Commun.*, vol. 13, no. 1, pp. 1–16, 2022, doi: 10.1038/s41467-022-33481-9.

[30] X. Shi, T. W. Liskiewicz, B. D. Beake, J. Chen, and C. Wang, "Tribological performance of graphite-like carbon films with varied thickness," *Tribol. Int.*, vol. 149, no. January 2019, p. 105586, 2020, doi: 10.1016/j.triboint.2019.01.045.

[31] L. Vergari, J. Quincey, G. Meric de Bellefon, T. Merriman, M. Hackett, and R. O. Scarlat, "Self-lubrication of nuclear graphite in argon at high temperature," *Tribol. Int.*, vol. 177, no. September 2022, p. 107946, 2023, doi: 10.1016/j.triboint.2022.107946.

[32] M. M. Rahman, M. Islam, R. Roy, H. Younis, M. AlNahyan, and H. Younes, "Carbon Nanomaterial-Based Lubricants: Review of Recent Developments," *Lubricants*, vol. 10, no. 11, pp. 1–28, 2022, doi: 10.3390/lubricants10110281.

[33] M. Dienwiebel, G. S. Verhoeven, N. Pradeep, J. W. M. Frenken, J. A. Heimberg, and H. W. Zandbergen, "Superlubricity of Graphite," *Phys. Rev. Lett.*, vol. 92, no. 12, p. 126101, Mar. 2004, doi: 10.1103/PhysRevLett.92.126101.